

Appendix C

Groundwater Numerical Modeling Support for the Idaho Nuclear Technology Engineering Center, Operable Unit 3-13, Group-5 Interim Action

[Editor's note: The document that is the subject of Appendix C, Groundwater Numerical Modeling Support for the Idaho Nuclear Technology Engineering Center, Operable Unit 3-13 Group-5 Interim Action, is available only as an Adobe Acrobat file (.pdf).]

Appendix C

**Groundwater Numerical Modeling Support for the Idaho
Nuclear Technology Engineering Center, Operable Unit
3-13 Group-5 Interim Action**

TABLE OF CONTENTS

1	INTRODUCTON	1
2	REVIEW OF THE WAG-3 OU 3-13 RI/BRA AQUIFER MODEL.....	2
2.1	OU 3-13 RI/BRA Aquifer Model Parameterization.....	2
2.2	OU 3-13 RI/BRA Aquifer Model Calibration.....	6
2.3	REVIEW OF IODINE-129 SOURCE TERM	16
2.4	REVIEW OF OU 3-13 RI/BRA IODINE-129 SIMULATION RESULTS	19
3	WAG-3 OU 3-13 RI/BRA AQUIFER MODEL SENSITIVITY TO INTERBED PARAMETERIZATION	34
3.1	HI Interbed Discretization Sensitivity.....	34
3.1.1	HI Interbed Placement	36
3.1.2	HI Interbed Rediscrctization	42
3.1.3	Model Discretization Sensitivity Results	43
3.2	Model Sensitivity to HI Interbed Permeability	48
3.2.1	Permeability Data Review.....	48
3.2.2	Permeability Sensitivity Results	49
4	WAG-3 UPDATED AQUIFER MODEL CALIBRATION AND PREDICTIVE SIMULATIONS	51
4.1	Updated Model Calibration.....	51
4.1.1	Aquifer Hydraulic Head Calibration.....	52
4.1.2	CPP-3 Injection Well Tritium Disposal Calibration	54
4.2	UPDATED MODEL PREDICTIVE SIMULATIONS.....	59
4.2.1	Iodine-129	61
4.2.2	Cobalt-60.....	66
4.2.3	Cesium-137	68
4.2.4	Tritium.....	72
4.2.5	Plutonium-241.....	77
4.2.6	Strontium-90	77
4.2.7	Technetium-99.....	83
4.2.8	Predictive Simulation Summary.....	87
5	MODELING DATA NEEDS.....	89
6	MODELING PATH FORWARD.....	90
7	REFERENCES.....	91

LIST OF FIGURES

2-1	Aquifer model domain	3
2-2	3-D Aquifer model representation	4
2-3	Wag 10 hydraulic conductivity zones and model domain.....	5
2-4	CPP-3 injection well actual and simulated tritium disposal data.....	8
2-5	RI/BRA simulated hydraulic head with spring 1999 observations.....	9
2-6	RI/BRA simulated hydraulic head with spring 1999 observations near the INTEC.....	10
2-7	Locations of RI/BRA tritium calibration wells.....	11
2-8	Locations of RI/BRA tritium calibration wells near INTEC.....	12
2-9	RI/BRA model tritium calibration wells breakthrough.....	13
2-10	I-129 actual and simulated disposal history to the aquifer from the CPP-3 injection well.....	18
2-11	I-129 actual and simulated disposal history to the vadose zone from the CPP-3 injection well.....	18
2-12	I-129 simulated mass flux from the vadose zone.....	19
2-13	RI/BRA model I-129 concentrations, TETRAD version 12.2 vs. 12.7 for layers 1-6 in 5/1959.....	21
2-14	RI/BRA model I-129 concentrations, TETRAD version 12.2 vs. 12.7 for layers 7-10 in 5/1959.....	22
2-15	RI/BRA model I-129 concentrations, TETRAD version 12.2 vs. 12.7 for layers 1-6 in 11/1972.....	23
2-16	RI/BRA model I-129 concentrations, TETRAD version 12.2 vs. 12.7 for layers 7-10 in 11/1972.....	24
2-17	RI/BRA model I-129 concentrations, TETRAD version 12.2 vs. 12.7 for layers 1-6 in 4/1992.....	25
2-18	RI/BRA model I-129 concentrations, TETRAD version 12.2 vs. 12.7 for layers 7-10 in 4/1992.....	26
2-19	RI/BRA model I-129 concentrations, TETRAD version 12.2 vs. 12.7 for layers 1-6 in 3/2025.....	27
2-20	RI/BRA model I-129 concentrations, TETRAD version 12.2 vs. 12.7 for layers 7-10 in 3/2025.....	28
2-21	RI/BRA model I-129 concentrations, TETRAD version 12.2 vs. 12.7 for layers 1-6 in 10/2095.....	29
2-22	RI/BRA model I-129 concentrations, TETRAD version 12.2 vs. 12.7 for layers 7-10 in 10/2095.....	30
2-23	RI/BRA model maximum I-129 concentrations in 2000 and 2095 with plume axis.....	31
2-24	RI/BRA model plume axis vertical I-129 concentrations in 1954, 1965, 1981, and 2000.....	32
2-25	RI/BRA model plume axis vertical I-129 concentrations in 2025, 2058, 2074, and 2095.....	33
3-1	INEEL deep wells locations with flowing aquifer depth.....	35
3-2	Updated aquifer model thickness.....	36
3-3	Simulated HI interbed thickness surface.....	39
3-4	Simulated HI interbed thickness surface in the INTEC vicinity.....	40
3-5	Simulated HI interbed surface elevation.....	41
3-6	Simulated HI interbed surface elevation in the INTEC vicinity.....	42
3-7	Updated aquifer model vertical discretization with vertical exaggeration.....	43
3-8	Rediscretized model maximum I-129 concentrations in 2000 and 2095 with plume axis.....	45
3-9	Rediscretized model plume axis vertical I-129 concentrations in 1954, 1965, 1981, and 2000.....	46
3-10	Rediscretized model plume axis vertical I-129 concentrations in 2025, 2058, 2074, and 2095.....	47
4-1	Initial H basalt hydraulic conductivity estimate.....	52
4-2	Rediscretized model hydraulic head with spring 1999 observations.....	53
4-3	Rediscretized model hydraulic head with spring 1999 observations near the INTEC.....	54
4-4	Updated model tritium calibration wells breakthrough.....	56
4-5	Well locations used for comparison of simulated and measured contaminant concentration.....	60
4-6	Well locations used for comparison of simulated and measured contaminant concentration near the INTEC.....	61
4-7	Peak aquifer concentration for I-129.....	62
4-8	Comparison of simulated and measured I-129 concentrations.....	63
4-9	Peak aquifer concentration for Co-60.....	66

4-10	Comparison of simulated and measured Co-60 concentrations.	67
4-11	Peak aquifer concentration for Cs-137.	68
4-12	Comparison of simulated and measured Cs-137 concentrations.	69
4-13	Peak aquifer concentration for H-3.	72
4-14	Comparison of simulated and measured H-3 concentrations.	73
4-15	Peak aquifer concentration for Pu-241.	77
4-16	Peak aquifer concentration for Sr-90.	78
4-17	Comparison of simulated and measured Sr-90 concentrations.	79
4-18	Peak aquifer concentration for Tc-99.	83
4-19	Comparison of simulated and measured Tc-99 concentrations.	84
4-20	Cumulative risk for all simulated COCs.	88
4-21	Cumulative dose rate for all simulated COCs.	88

LIST OF TABLES

2-1	WAG-10 permeability and hydraulic conductivity in the vicinity of the INTEC.	5
2-2	Summary of the I-129 sources and time frame of environmental and aquifer flux.....	17
2-3	Maximum I-129 concentrations predicted with TETRAD version 12.2 and 12.7.....	20
3-1	HI interbed elevation and thickness data.....	37
3-2	Summary of interbed hydraulic conductivity data from the OU 3-13 RI report.....	48
3-3	Summary of calibrated HI interbed permeability values.....	49
3-4	Permeability sensitivity year 2095 I-129 maximum concentrations and areal extent.....	50
4-1	Simulated beta/gamma radiation emitting contaminants.	59
4-2	Predictive simulation peak aquifer concentrations.....	87

Appendix C

Groundwater Numerical Modeling Support for the Idaho Nuclear Technology Engineering Center, Operable Unit 3-13 Group-5 Interim Action

1 INTRODUCTION

Modeling of the Snake River Plain Aquifer for the WAG-3 (Waste Area Group 3) Operable Unit (OU) 3-13 Remedial Investigation/Baseline Risk Assessment (RI/BRA) (DOE-ID, 1997) predicted a risk beyond the year 2095 to groundwater users due to groundwater concentrations of I-129 and Sr-90 predicted to remain in the low-hydraulic conductivity HI sedimentary interbed. However, only a limited amount of empirical data is available to confirm the physical properties of the HI interbed as assumed in the OU 3-13 RI/BRA model and there is no data regarding the presence or absence of contaminants in the interbed. Empirical evidence of the HI interbed contamination and permeability is required to verify the model predictions and refine the model parameterization.

Sensitivity of the model parameterization was performed to identify key data needs and support field activities to collect empirical data. The Iodine 129 isotope (I-129) was chosen as the indicator contaminant for model sensitivity because it is long lived and it was predicted to present the greatest long term risk within the interbed. A refined and recalibrated model was then used to determine if contamination within the HI interbed still presents a risk to groundwater users. The refined and recalibrated model represents a first effort in updating the WAG-3 conceptual model with more recent data. However, the new model needs to incorporate data from the HI interbed sampling/characterization effort before the predictive simulations can be relied upon.

The tasks performed to refine the model and to assess sensitivity were: (1) review of the OU 3-13 RI/BRA model, (2) review of the I-129 source term in the model, (3) review of the existing HI interbed thickness and elevation data, (4) rediscretization of the OU 3-13 RI/BRA (hereafter referred to as “rediscretized”) model to include all the existing interbed data, (5) sensitivity analysis of HI interbed discretization, (6) review of the HI interbed permeability data, (7) sensitivity analysis of HI interbed permeability, (8) recalibration of the rediscretized model (hereafter referred to as “updated”), and (9) predictive simulations with the updated model for the beta/gamma radiation emitting contaminants of concern (COCs) identified in the RI/BRA. The predictive simulations were performed to assess the cumulative aquifer risk and estimate concentrations of other radionuclides, which may need to be addressed if remediation is needed.

The results of performing these tasks are documented in this report. Section 2 presents a review of the RI/BRA aquifer model and the I-129 simulations. Section 3 presents the sensitivity analysis of the HI interbed parameterization. Section 4 presents the updated model calibration and predictive simulations. Section 5 presents modeling data needs, and Section 6 provides a modeling path forward.

2 REVIEW OF THE WAG-3 OU 3-13 RI/BRA AQUIFER MODEL

The OU 3-13 RI/BRA modeling was performed using the TETRAD multi-purpose simulator (Vinsome and Shook, 1993). Two separate models were used to represent the vadose zone and aquifer beneath the Idaho Nuclear Technology Engineering Complex (INTEC). The basis for these two conceptual models are briefly presented here. A detailed description of the OU 3-13 RI/BRA models can be found in Appendix F, DOE-ID (1997).

2.1 OU 3-13 RI/BRA Aquifer Model Parameterization

The physical and hydrogeologic setting of the INTEC is highly complex, consisting of layers of basalt and sediments. In the vadose zone, the sedimentary interbeds are often saturated, forming perched water zones. The geology of the aquifer region is more uniform in the vertical direction than the geology of the vadose zone. The aquifer basalt structures tend to be thicker, and the sedimentary interbeds are fewer in number. USGS studies (Anderson, 1991) indicate that aquifer in the region north of the INTEC and extending south of the RWMC is comprised primarily of the H basalt flow, the HI interbed, and the I basalt flow. The I basalt flow is significantly thicker (Anderson, 1991) and may have a lower permeability than the H basalt flow because the high permeability inter-flow rubble zones represent a smaller fraction of the total flow thickness. The HI interbed separates the two basalt flows.

The RI/BRA aquifer model incorporated the I basalt flow, the HI interbed, and the H basalt flow. The aquifer model domain extends from approximately 2.5 km north of the INTEC facility to the southern INEEL boundary in the north-south direction and approximately 6.5 km east of the INTEC facility to slightly west of the RWMC facility in the east-west direction. The model was discretized into 400 x 400 x 7.6 m grid blocks as shown in Figures 2-1 and 2-2. Local refinement corresponding to the discretization level applied in the vadose zone model is used for the footprint of the INTEC (200 x 200 m grid) and also in the vicinity of TRA. This local refinement was only in the top 7.6 m of the aquifer model.

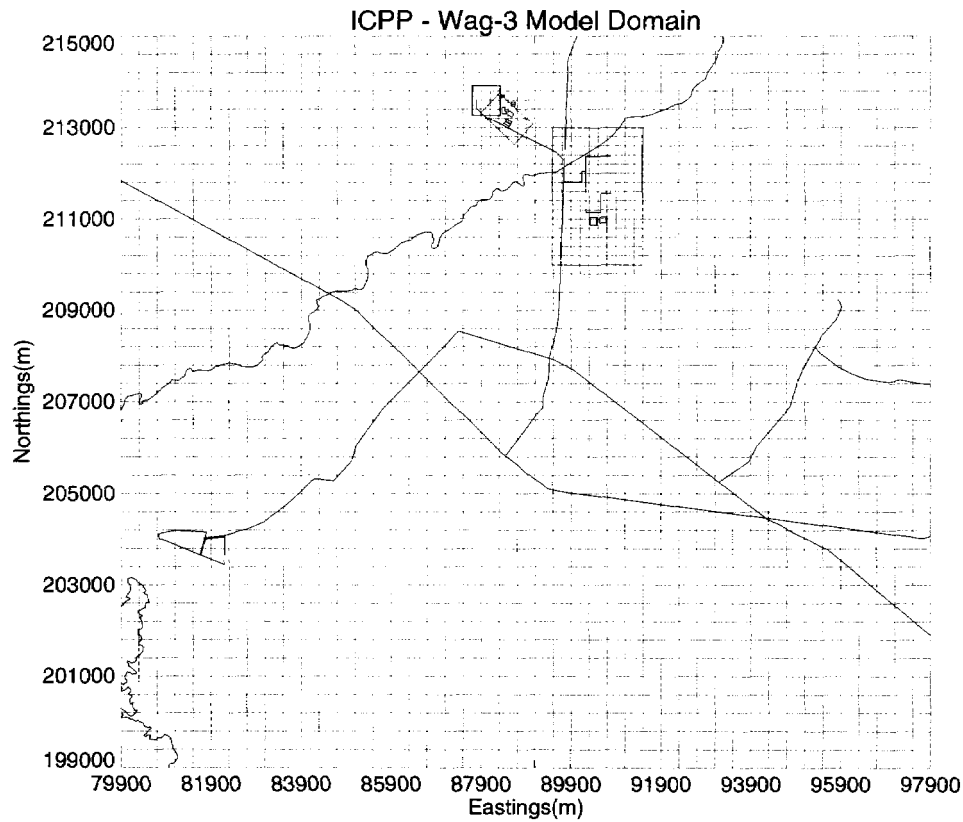


Figure 2-1 Aquifer model domain.

The vertical aquifer domain extends downward from an elevation of 1,360 m to 1,284 m. This total depth was chosen to be below the completion intervals of the primary INTEC pumping and injection wells and from the effective aquifer thickness estimated by Robertson (1974).

The aquifer model used four distinct stratigraphic types. These include an upper I basalt unit, a lower I basalt unit, the HI interbed, and the H basalt. The upper I basalt structure was assigned permeabilities representative of those obtained from aquifer testing of the INTEC pumping and injection wells. The lower I basalt and H basalt structure used regional permeabilities taken from the WAG-10 modeling effort (McCarthy et al., 1995). The H basalt structure in the vicinity of the vadose zone foot print was assigned local INTEC permeabilities from the pumping tests.

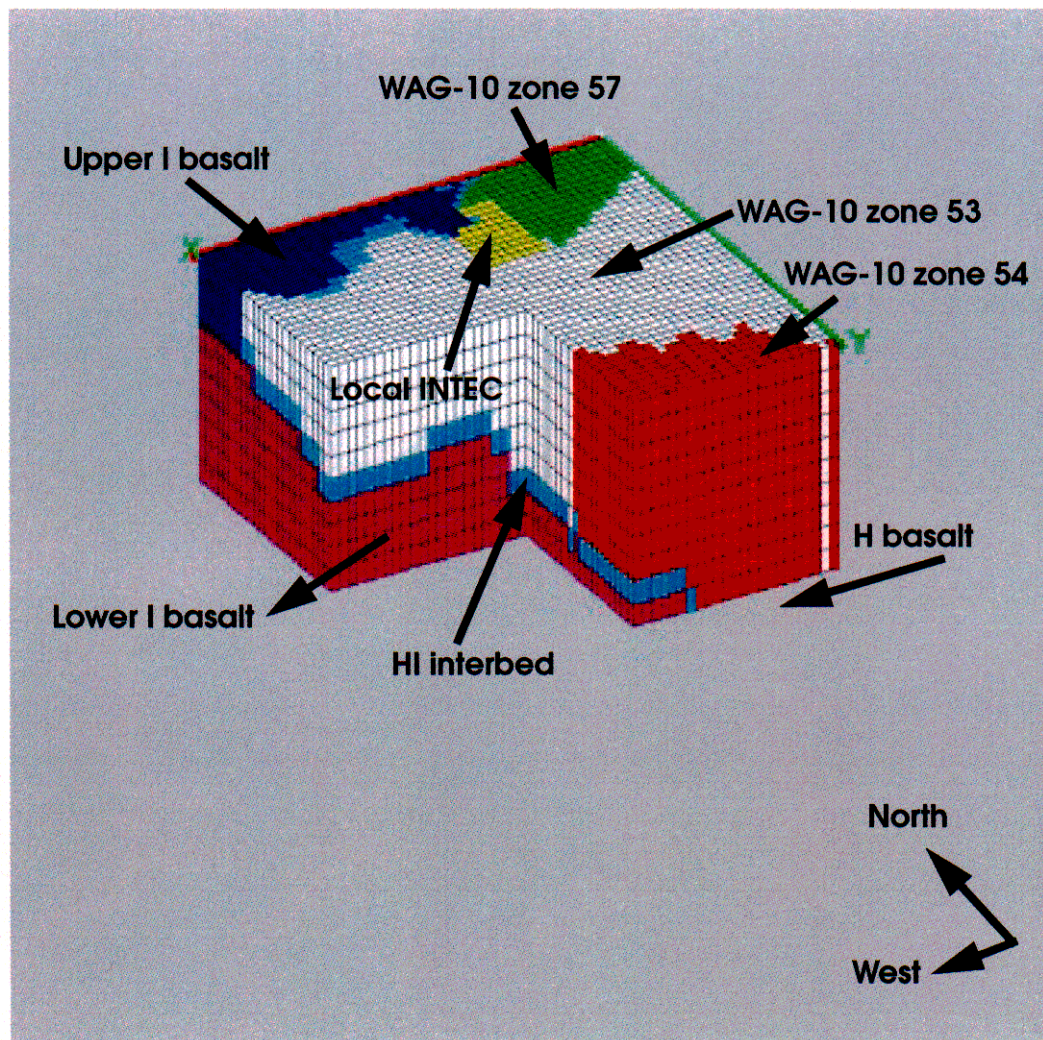


Figure 2-2 3-D Aquifer model representation

The I basalt flow, HI interbed and H basalt unit were combined into a three-dimensional domain by preserving the I basalt flow top and assumed thickness to the bottom of our modeling domain. As illustrated in Figure 2-2, the I basalt flow rises above the water table along the north to northwest boundary. The slope of the I basalt flow near the north west of the region shown is steeply angled downward. High dip angles may be associated with more fractures which means that the top of the I basalt flow will exhibit higher permeability, with the permeability decreasing in the flatter regions to the south. This distinction between an upper and lower I basalt region is indicated by dark blue and violet shades in Figure 2-2, respectively. The turquoise shade region represents the HI sedimentary interbed. The vertical discretization throughout the model is uniform at a spacing of 7.6 m. The uniform vertical discretization fixes the HI interbed to be 7.6 m thick.

The hydraulic conductivities used in the aquifer model were first interpolated onto the WAG-3 model grid from the WAG 10 regional groundwater flow model. This model used an Eastern Snake River Plain regional water balance to define the boundaries in order to ensure a water mass balance through the Eastern Snake River Plain aquifer. The permeabilities used in the WAG 10 model are shown in Figure 2-3 and given for the INTEC region in Table 2-1.

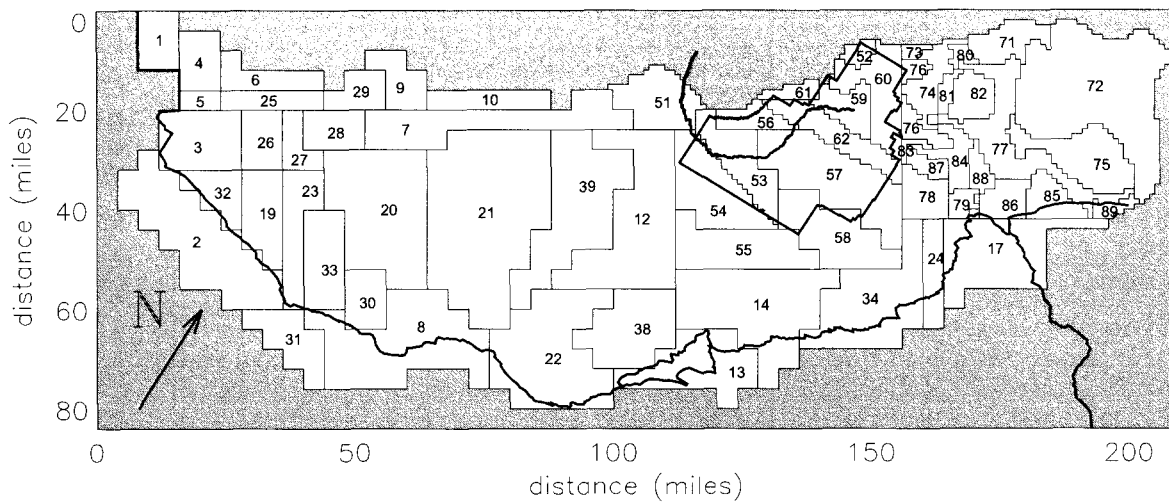


Figure 2-3 Wag 10 hydraulic conductivity zones and model domain.

Table 2-1 WAG-10 permeability and hydraulic conductivity in the vicinity of the INTEC.

WAG 10 K Zone	Permeability (mD)	Hydraulic Conductivity (ft/day)	Comment
53	170,000	459	INTEC is in this zone
54	1,800,000	4,925	This zone is south of the INTEC.
57	370,000	1,002	This zone is east of the INTEC.

The upper I basalt unit, lower I basalt unit, and the HI interbed are the dominant stratigraphic features in the saturated zone. It is hypothesized that the upper I basalt flow and lower I basalt flow differ hydraulically because the I basalt flow dips steeply near the north to northwest boundary of our model domain. This dip means that the top of that basalt flow is probably more highly fractured and thus exhibits higher permeability, with the permeability decreasing in the flatter regions to the south. Distinguishing an upper and lower I basalt region was done by assigning a value representative of the permeabilities taken from pumping tests of wells CPP-01, CPP-02, and CPP-3 to the upper I basalt region, and assigning one half of the lowest WAG-10 INTEC permeability (8.5×10^4 mDarcy) to the lower I basalt region. These values replaced the WAG-10 permeabilities in grid blocks containing the I basalt flow.

To be consistent with the sediment properties used in the vadose zone interbeds, a permeability of 4 mD (0.01 ft/day) and porosity of 0.487 was assigned to the first layer of grid blocks overlying the I basalt flow. The vadose zone interbed permeability was determined by calibrating to perched water depth in the vadose zone. Assigning sediment properties uniformly over the I flow assumed that the HI interbed is 7.6 m thick and exists everywhere the I basalt flow is below the water table. The porosity for the aquifer model basalt was 0.0625. This value was derived from calibration of the aquifer model to tritium disposal records and the corresponding tritium sampling results from wells in the vicinity of and down gradient of the INTEC.

The final level of refinement for basalt hydraulic conductivities in the INTEC aquifer model was to incorporate INTEC local scale field data. These local scale hydraulic conductivities were initially applied

throughout the vertical profile defined by the footprint of the vadose zone model. These values were then slightly adjusted by setting a minimum value at 18,000 mD to prevent excessive mounding beneath the Big Lost River.

The Big Lost River flows across the aquifer model domain and infiltration from the Big Lost River was applied directly in the aquifer model outside the area of the vadose zone footprint. Infiltration within the footprint was accounted for indirectly through the water flux from the vadose zone model. In addition to the Big Lost River, there are three other primary water sources influencing the aquifer heads. These were pumping from CPP-01, CPP-02 and CPP-04; reinjection into CPP-03; and recharge from percolation ponds. The pumping and injection wells were simulated in the aquifer model. Water from the percolation ponds was accounted for indirectly from the vadose zone model flux.

The boundary conditions for the aquifer model were specified flux at the surface, which included the water sources discussed above, no flux at the bottom, and specified heads on the sides. The specified heads were interpolated from the WAG-10 model.

2.2 OU 3-13 RI/BRA Aquifer Model Calibration

The OU 3-13 RI/BRA aquifer flow model relied on the WAG-10 model calibration (McCarthy et al., 1994) and the hydraulic parameters were not adjusted in the transport calibration process. Calibration of the transport model parameters (porosity and dispersivity) used the tritium disposal history in the CPP-03 injection well. The tritium disposed in CPP-03 provided fair calibration data because the inventory disposed to the injection well is fairly well defined and there is a long historical record (1953-present) from USGS wells located down gradient. Figure 2-4 illustrates the CPP-3 injection well tritium disposal history used in the RI/BRA aquifer model calibration. A more detailed description of the RI/BRA tritium calibration can be found in Appendix F, DOE-ID (1997).

The match between RI/BRA simulated hydraulic head and tritium concentrations and the observed values was evaluated with both qualitative and quantitative criteria. The RI/BRA model agreement with observed values has been assessed to provide a standard for calibration of the updated aquifer model. The qualitative criteria included simulated contour maps of the spring 1999 hydraulic head measurements with observed data plotted on the maps, and simulated tritium breakthrough curves at USGS observation wells with observed tritium concentrations overplotted on the curves. The spring 1999 hydraulic head measurements were chosen to evaluate the flow model because this data set is more comprehensive for a single time period than the data sets available when the RI/BRA modeling was performed.

Three quantitative indicators were chosen to measure the agreement between field data and simulation results: (1) the root mean square (RMS) error, (2) a modified version of the root mean square (ModRMS) error, and (3) the correlation coefficient. The RMS error was used to evaluate the match between observed and simulated hydraulic head. The RMS error provides a good estimation of the average error throughout the data set and is defined as:

$$RMS = \sqrt{\frac{\sum_{i=1}^k (s_i - f_i)^2}{k}} \quad (1)$$

where

f_i = field data point

s_i = simulation data point

k = number of comparison points.

The ModRMS error was used to evaluate the match between observed and simulated tritium concentrations. The modification was to divide the RMS error by the average measured tritium concentration at each observation well, over the observation period at each well. The modification allows distal wells with much lower tritium concentrations to have a similar weight on the overall RMS error as the near wells which have tritium concentrations several orders of magnitude higher. The more traditional relative mean square error (i.e., the error term $s_i - f_i$ in Equations 1 and 2 is replaced by $(s_i - f_i)/f_i$) could not be used because tritium concentrations are zero before and after the breakthrough and result in division by zero. Smaller values of the ModRMS error indicate a better agreement between simulated and observed values. The ModRMS error is most useful for comparing the performance of the updated model with the RI/BRA model. The ModRMS is defined as:

$$ModRMS = \frac{\sqrt{\frac{\sum_{i=1}^k (s_i - f_i)^2}{k}}}{\frac{\sum_{i=1}^k f_i}{k}} \quad (2)$$

The correlation coefficient was used to evaluate the agreement of the simulated and observed tritium breakthrough curve shape. The correlation coefficient measures the degree to which there is a linear correlation between two data sets. A perfectly linear relationship between data sets would result in a correlation coefficient of 1. Independent data sets would have a correlation coefficient of 0. Data sets which have a linear relationship, but trend in different directions will have a negative correlation coefficient. The correlation coefficient (r) is defined as:

$$r = \frac{k \sum_{i=1}^k s_i f_i - \sum_{i=1}^k s_i \sum_{i=1}^k f_i}{\sqrt{\left[k \sum_{i=1}^k s_i^2 - \left(\sum_{i=1}^k s_i \right)^2 \right] \left[k \sum_{i=1}^k f_i^2 - \left(\sum_{i=1}^k f_i \right)^2 \right]}} \quad (3)$$

The RI/BRA model's hydraulic head RMS error over all wells within the model domain was 1.6 m. The RI/BRA model's steady-state flow field with spring 1999 measured hydraulic head is presented in Figures 2-5 and 2-6. The RI/BRA model's tritium breakthrough average ModRMS error over all monitoring wells was 1.98 and the average correlation coefficient of all the calibration wells was 0.239. The ModRMS and correlation coefficient were calculated at the model grid block closest to the well screen center. Figures 2-7 and 2-8 illustrates the locations of the tritium breakthrough calibration wells and Figure 2-9 illustrates model predicted breakthrough and observed tritium concentrations for each well. Wells outside of the observed CPP-3 injection well tritium plume and wells with less than observed 2 data points were excluded from the ModRMS error and correlation coefficient calculation and Figure 2-9. Four data sets are plotted on each well's breakthrough plot: (1) observed concentration (thin black line with a cross data symbol), (2) simulated well screen center (thick red line), (3) simulated concentration at the aquifer top (thin dashed green line), and (4) simulated concentration at the aquifer bottom (thin blue line).

Two problems can be seen in the tritium disposal and breakthrough data sets. The first problem is tritium disposal prior to 1962 was reported as an annual average and the disposal data after 1962 suggests there may have been significant monthly variation in tritium disposal. The second problem is the highest observed tritium concentration in wells nearest the injection well (USGS-47, USGS-43, and USGS-41) occurs in 1962

while the disposal history indicates very little tritium was disposed during this time. Given the close proximity of these wells to the CPP-3 injection well and relatively high aquifer velocity, tritium disposal spikes should be almost immediately seen in the nearest down gradient wells.

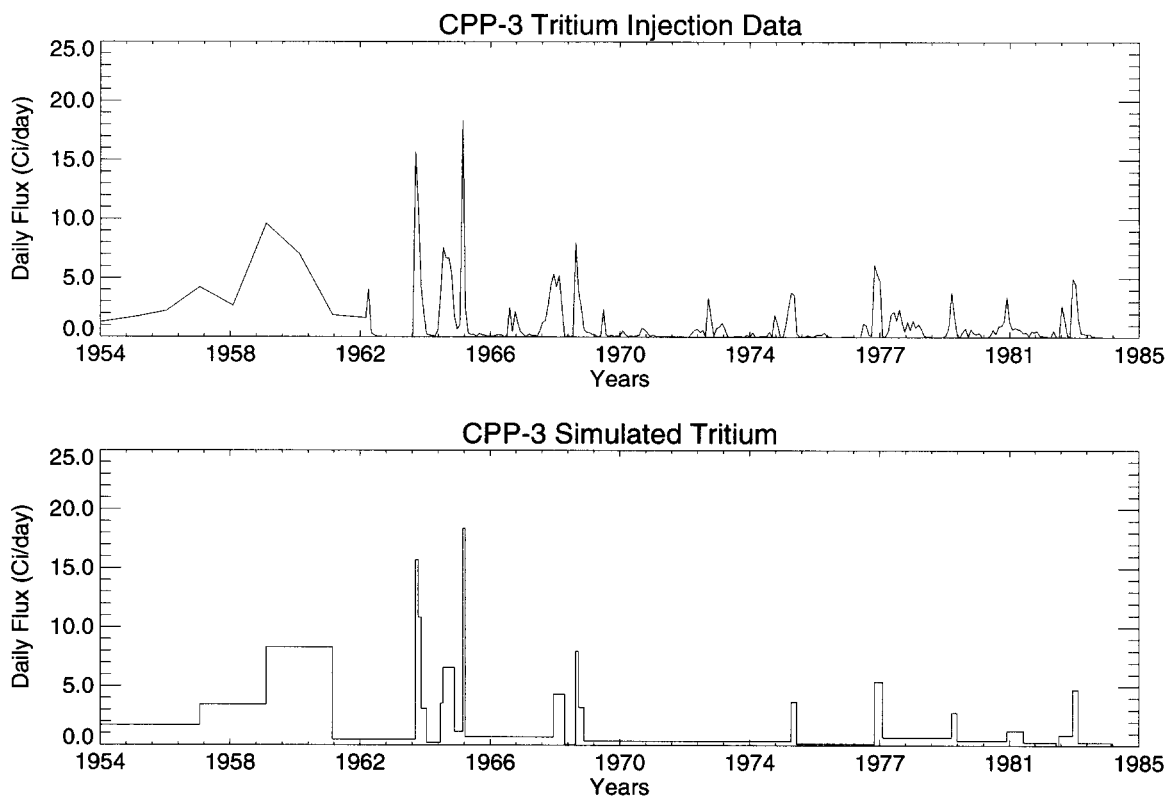


Figure 2-4 CPP-3 injection well actual and simulated tritium disposal data.

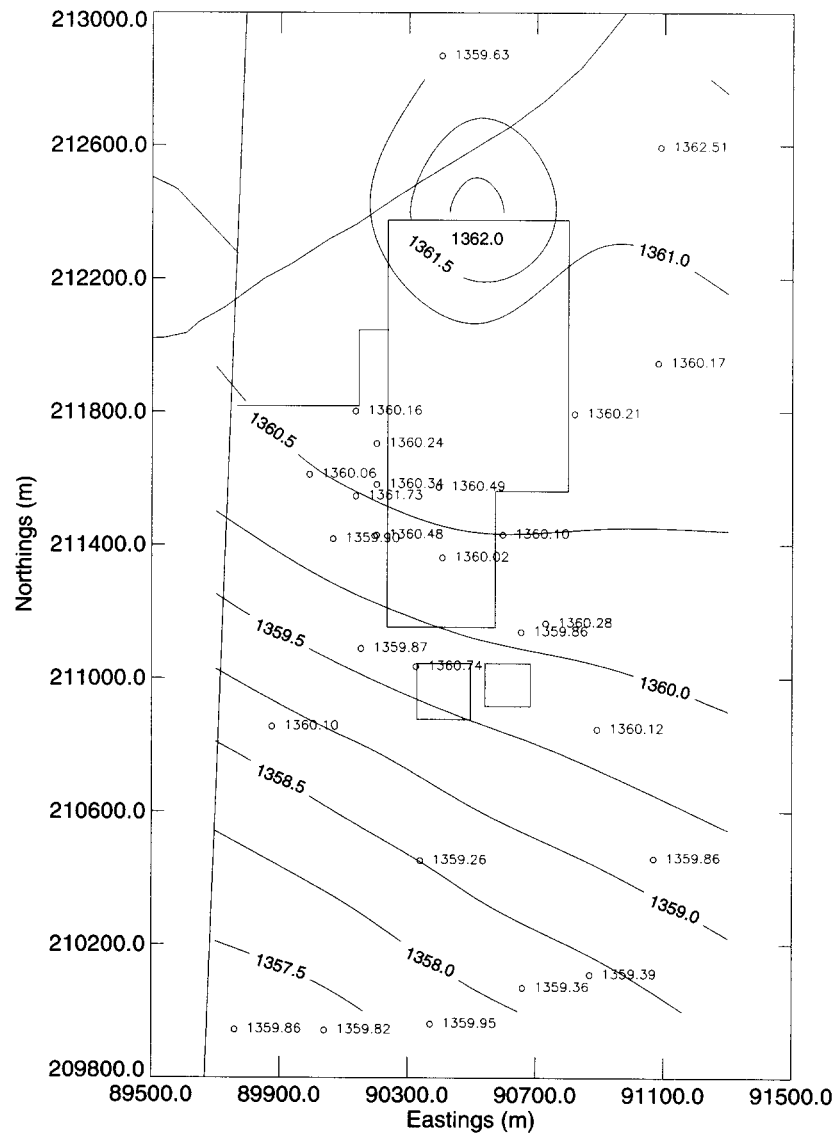


Figure 2-6 RI/BRA simulated hydraulic head (m) with spring 1999 observations near the INTEC.

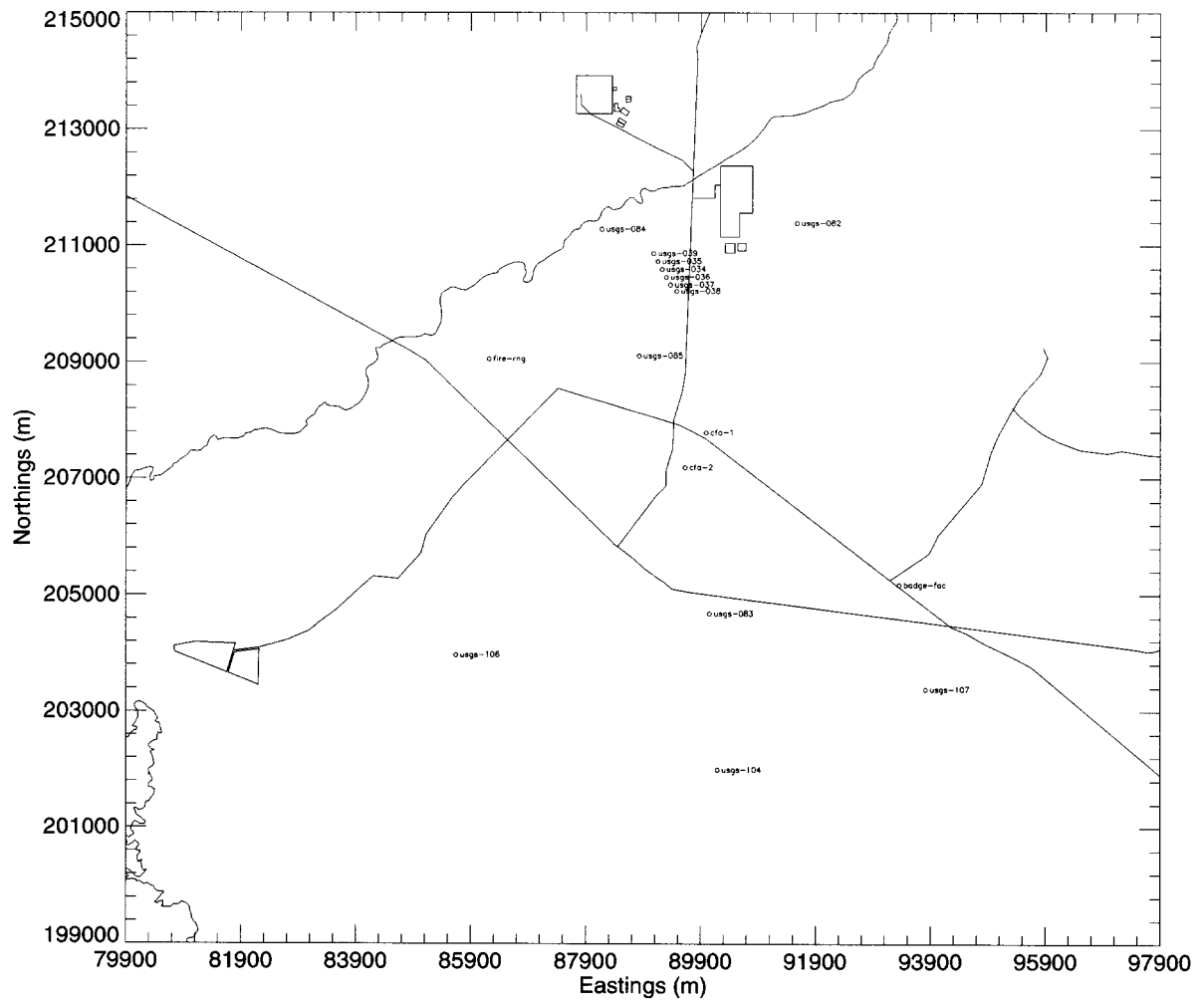


Figure 2-7 Locations of RI/BRA tritium calibration wells.

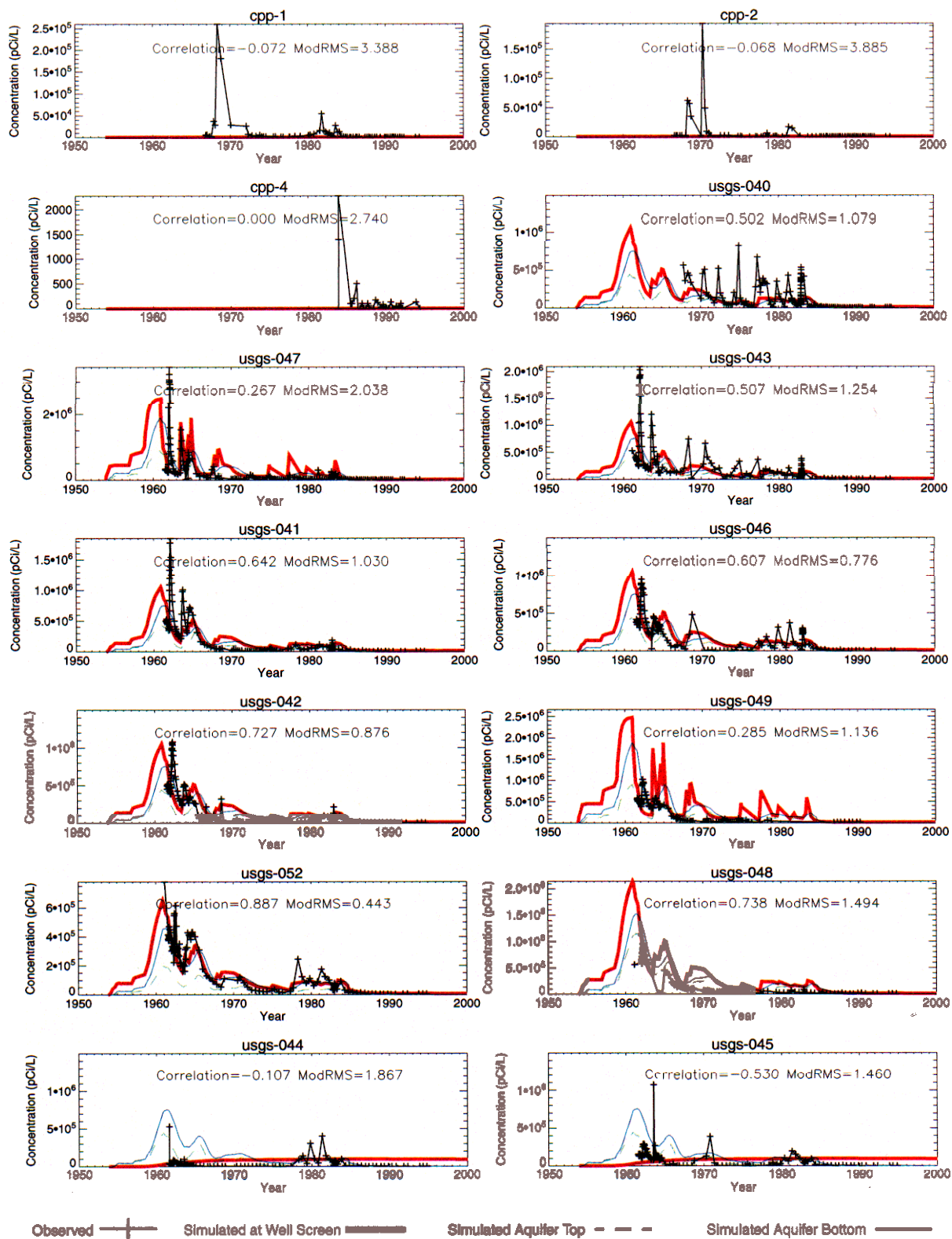


Figure 2-9 RI/BRA model tritium calibration wells breakthrough.

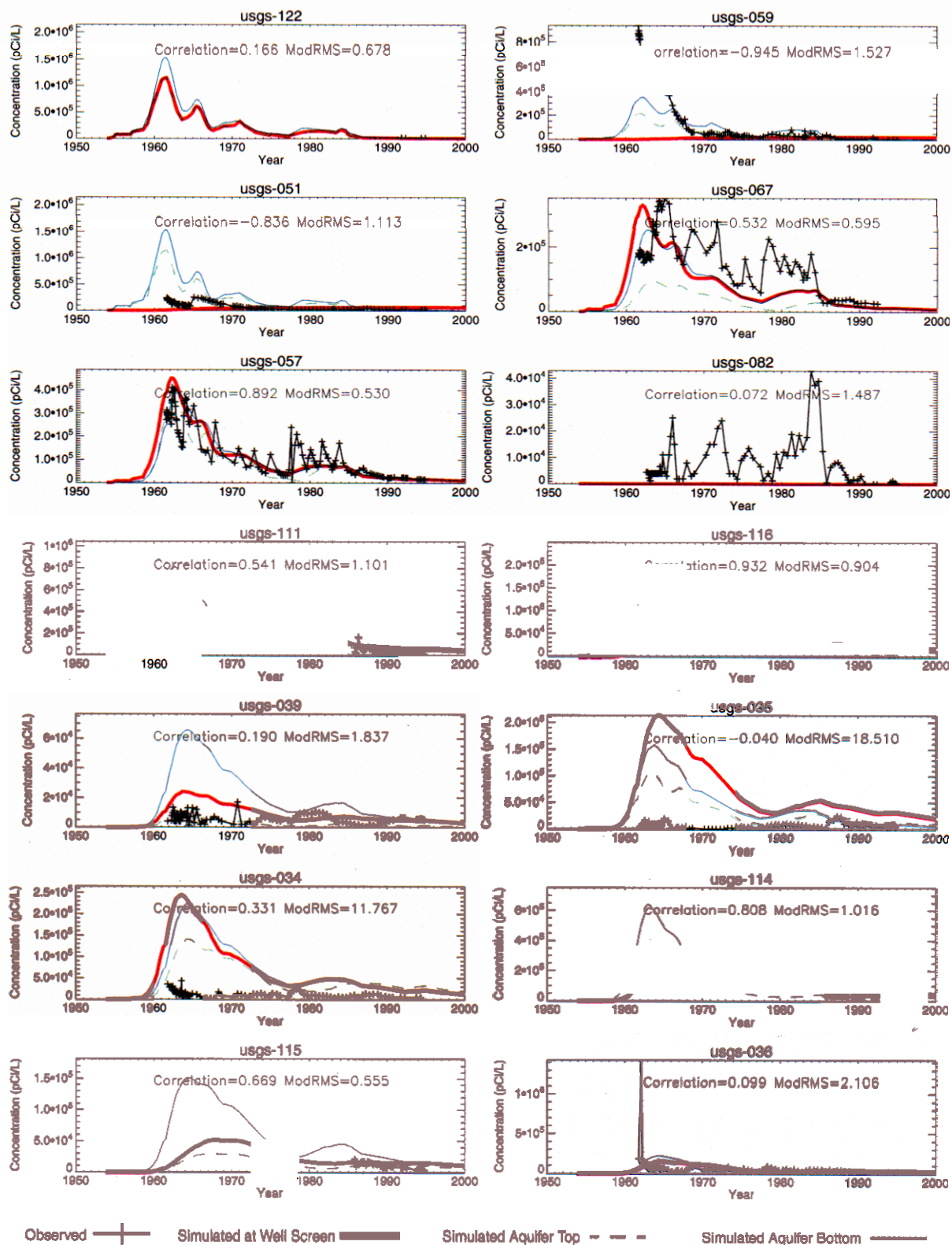


Figure 2-9 continued RI/BRA model tritium calibration wells breakthrough.

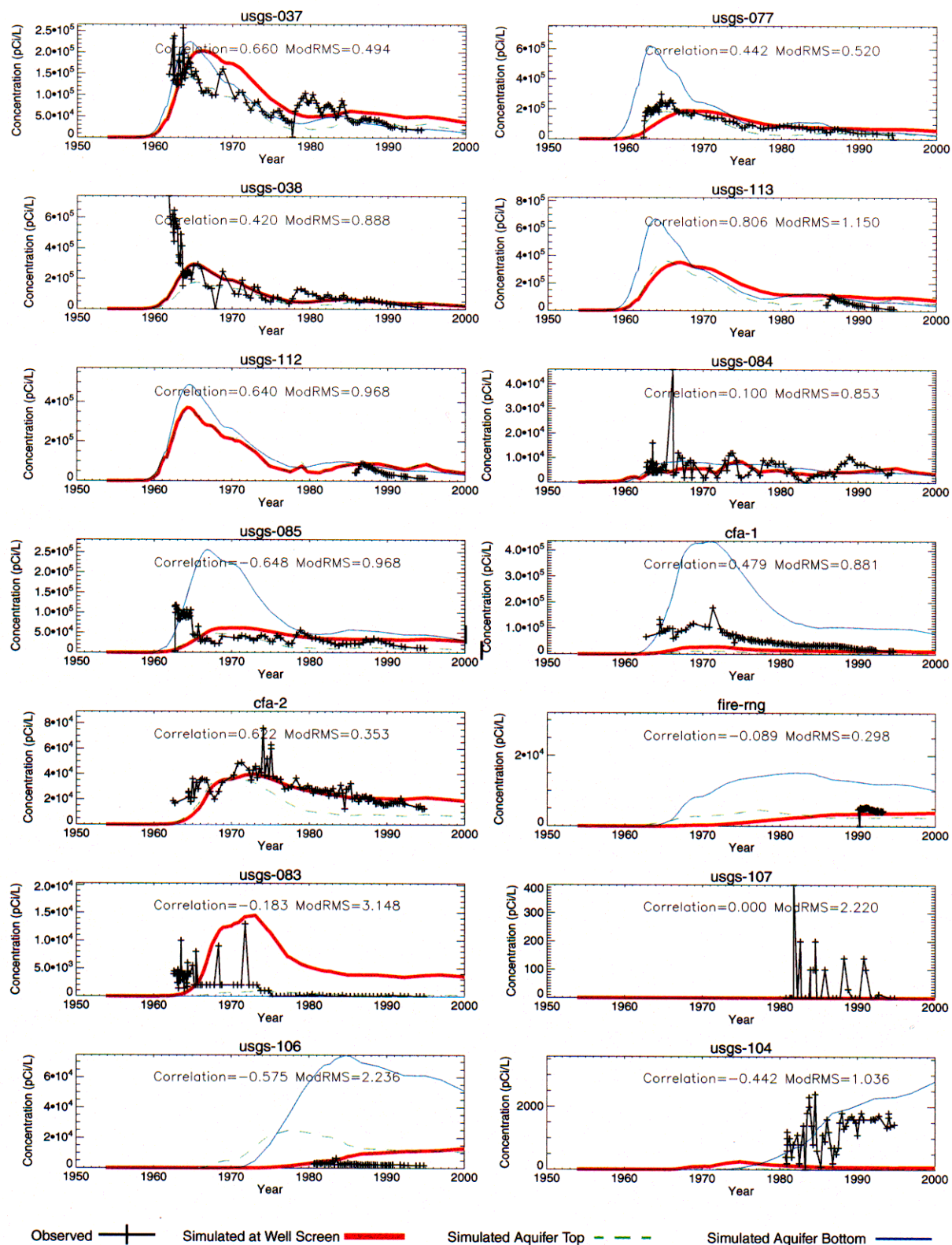


Figure 2-9 continued RI/BRA model tritium calibration wells breakthrough.